Supporting Information for

Lithophilic SiO_2 Nanoparticle Pillared MXene Nanosheets for Stable and Dendrite-Free Lithium Metal Anodes

*Shuaiqi Wang, Yaru Li, Xiaoze Zhou, Yi Yang, and Gang Chen**

School of Physical Science and Technology, ShanghaiTech University, Shanghai 201210, China

*E-mail: gchen@shanghaitech.edu.cn

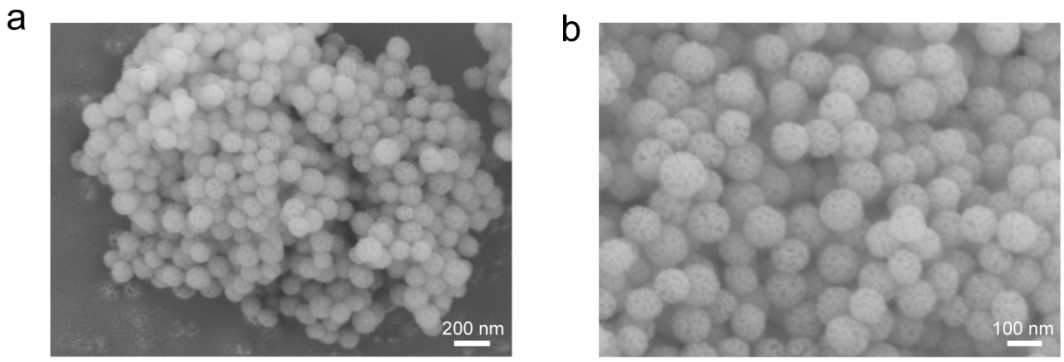

Figure S1. (a) Low magnification and (b) High magnification SEM images of SiO_2 nanoparticles. The diameter of SiO_2 nanoparticles is about 200 nm.

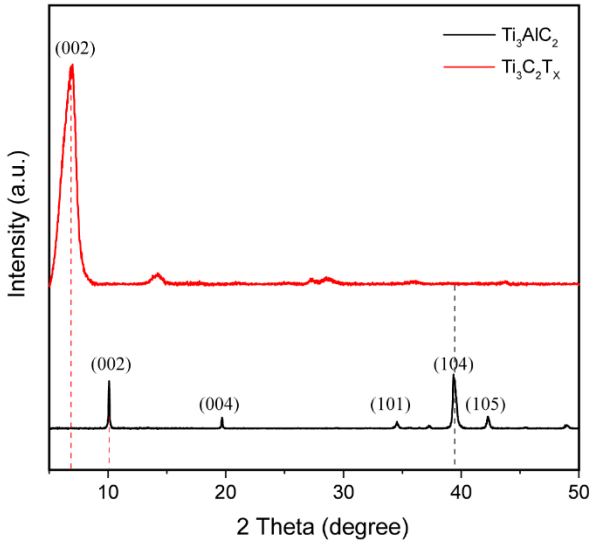

Figure S2. XRD patterns of MAX phase (Ti_3AlC_2) and MXene ($Ti_3C_2T_x$).

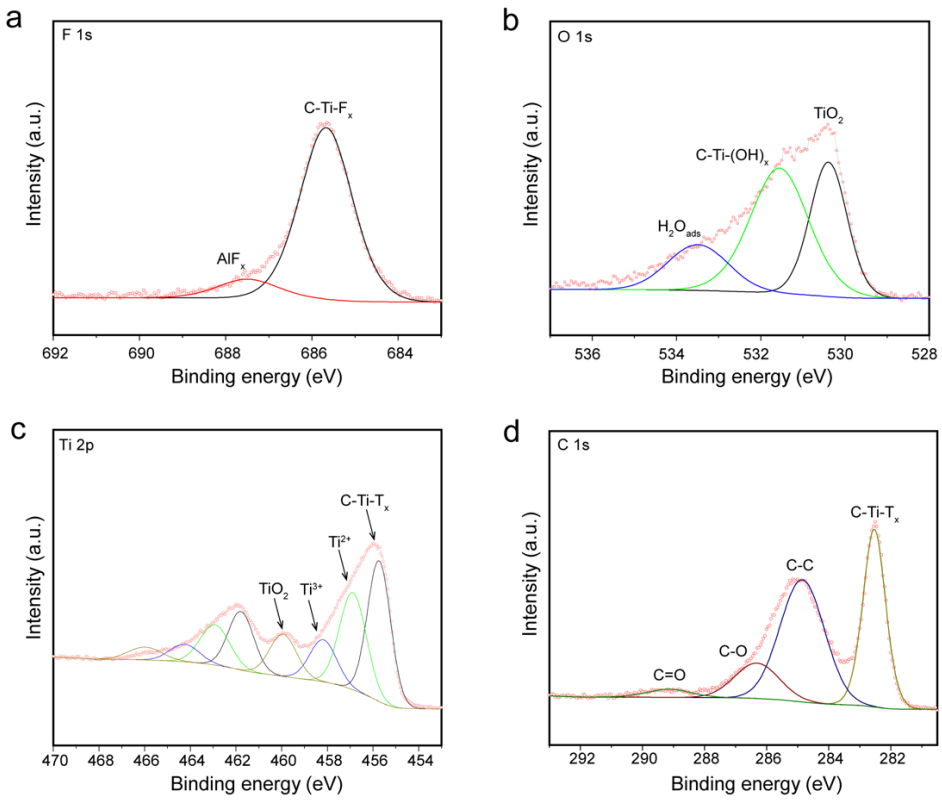

Figure S3. XPS characterization of MXene nanosheets. (a) F 1s, (b) O 1s, (c) Ti 2p, (d) C 1s.

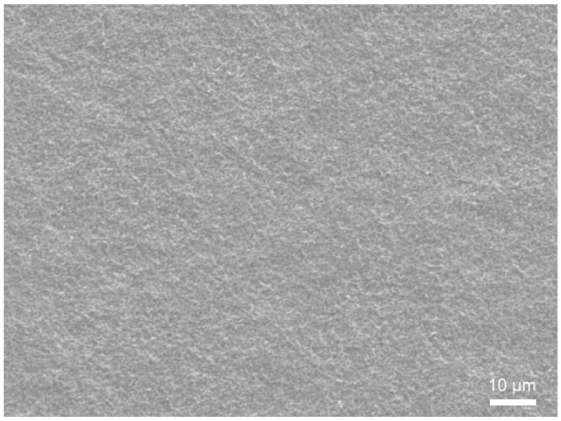

Figure S4. SEM image of the surface of the MXene/SiO_2 composite film.

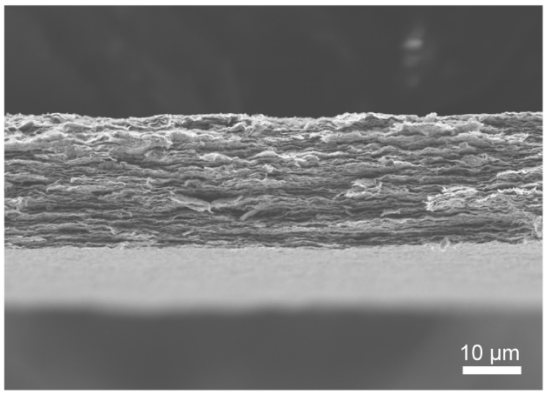

Figure S5. Cross-sectional SEM image of the MXene/SiO_2 composite film.

$$5\ SiO_2 + 4\ Li^+ + 4\ e^- \rightarrow 2\ Li_2Si_2O_5 + Si \quad \text{(S6 a)}$$

$$2\ SiO_2 + 4\ Li^+ + 4\ e^- \rightarrow Li_4SiO_4 + Si \quad \text{(S6 b)}$$

$$Si + x\ Li^+ + x\ e^- \rightarrow Li_xSi \quad \text{(S6 c)}$$

Figure S6. The electrochemical reactions of SiO_2 with Li.[1,2]

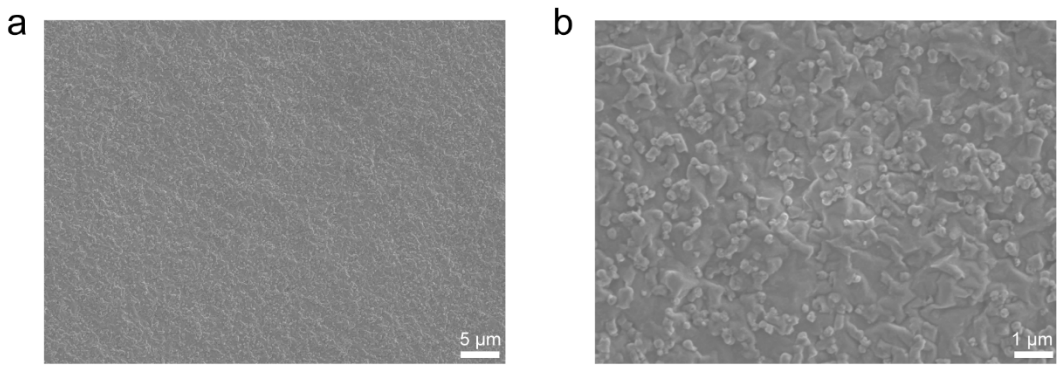

Figure S7. (a) Low magnification and (b) High magnification SEM images of the surfaces of the MXene/SiO_2 electrode after 10 cycles.

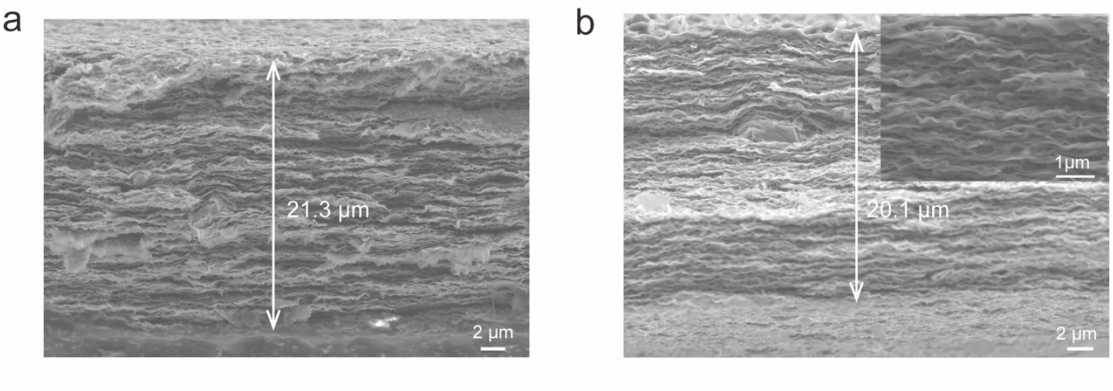

Figure S8. The cross-sectional SEM images of the MXene/SiO_2 composite film (a) at the initial state and (b) after 50 cycles of Li plating/stripping with the areal capacity of 3 mAh cm^{-2}. The inset shows the zoomed-in cross-sectional SEM image.

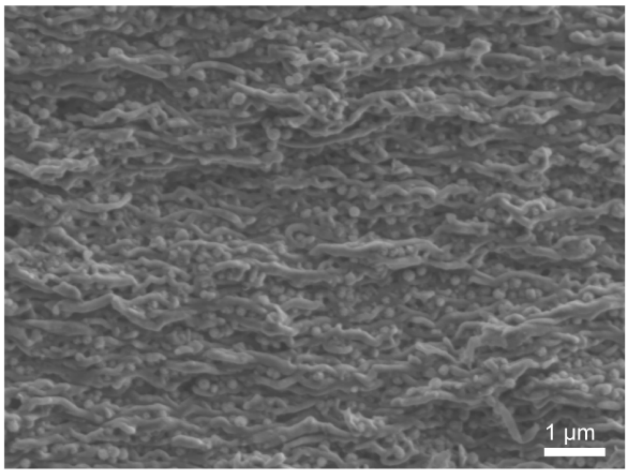

Figure S9. Cross-sectional SEM image of the MXene/SiO_2 electrode after Li plating at the capacity of 3 mAh/cm^2.

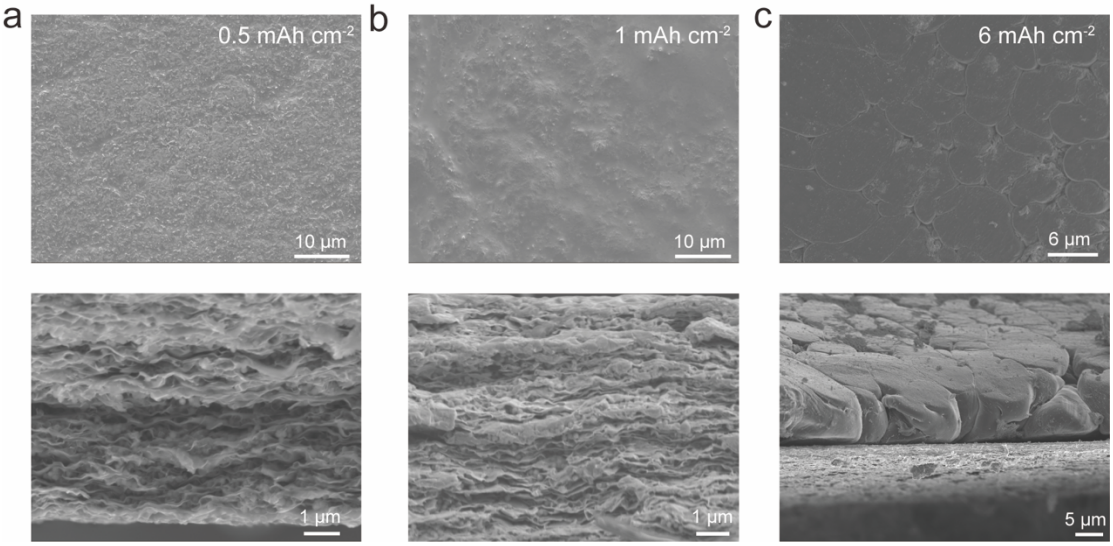

Figure S10. Top-view and cross-sectional SEM images of the MXene/SiO_2 films taken for different Li deposition capacities of (a) 0.5 mAh cm^{-2} , (b) 1 mAh cm^{-2}, (c) 6 mAh cm^{-2}. Li is preferentially deposited inside the MXene/SiO_2 films when the areal capacity is small. At sufficiently large capacity, Li starts to deposit on the surface of the MXene/SiO_2 film.

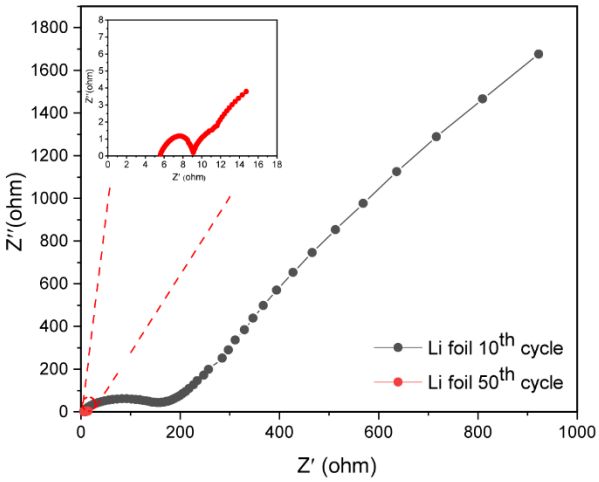

Fig S11. EIS spectra of the Li-Cu half cell taken at 10th and 50th cycles. The inset shows the zoomed-in view of the EIS spectrum recorded at 50th cycle.

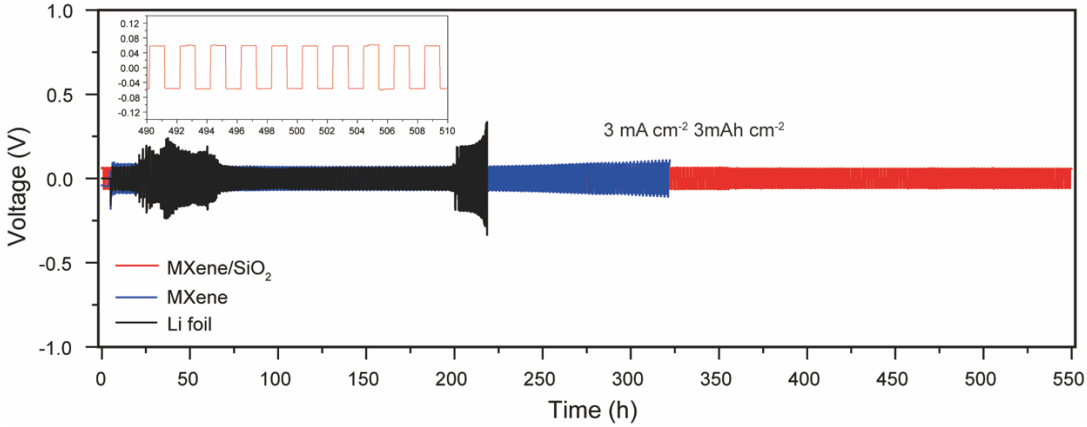

Fig S12. The cycling performance of the symmetric cells with the areal capacity of 3 mAh cm^{-2} at the current density of 3 mA cm^{-2}. The inset shows the zoomed-in profile from 490 to 510 h.

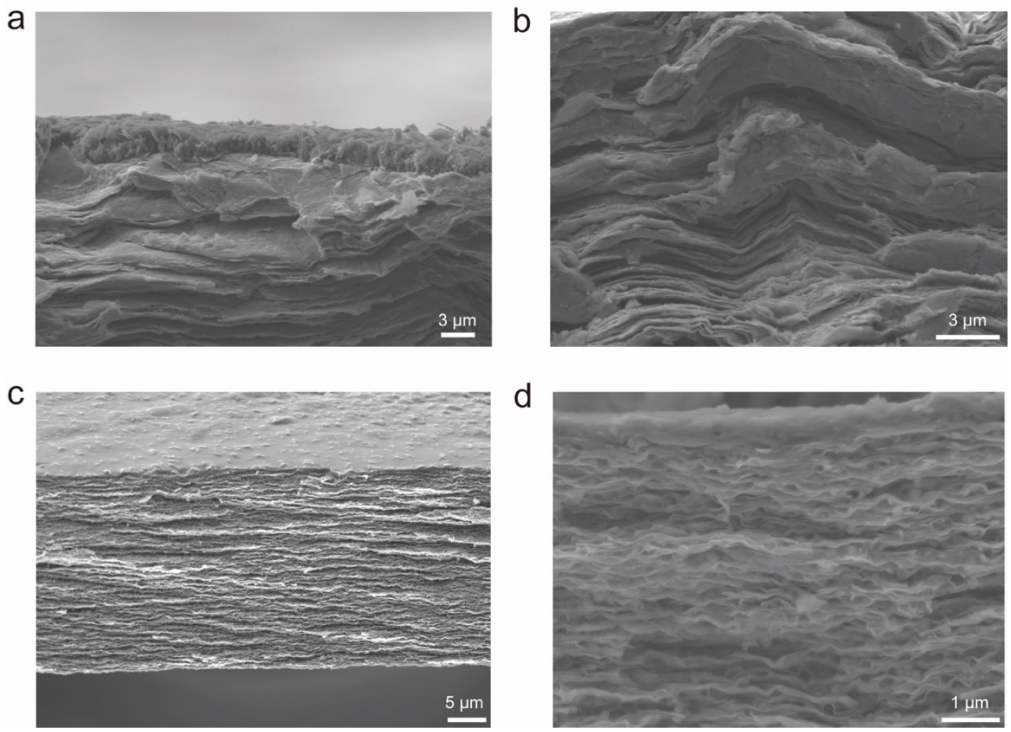

Fig S13. The cross-sectional SEM images of the MXene and MXene/SiO_2 films after cycling in the symmetric cells for 200 h with the areal capacity of 2 mAh cm^{-2} at 2 mA cm^{-2}. (a) Low magnification and (b) High magnification cross-sectional SEM images of the MXene film. (c) Low magnification and (d) High magnification cross-sectional SEM images of the MXene/SiO_2 film

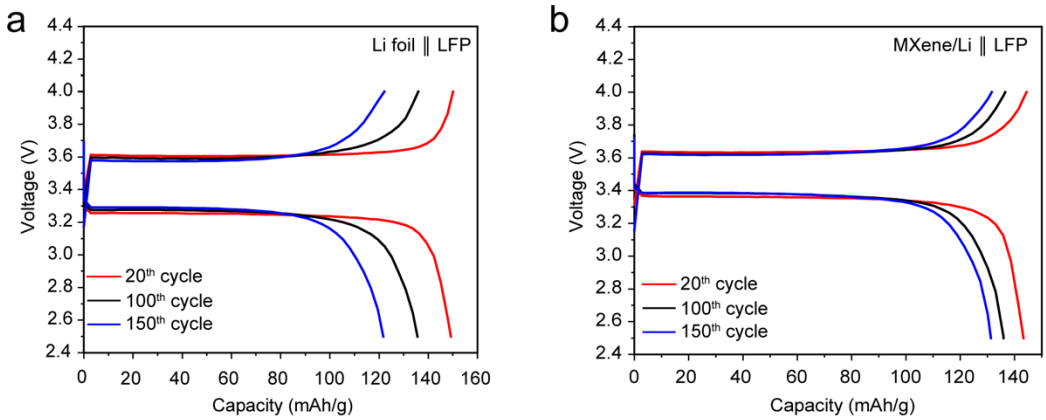

Figure S14. The charge–discharge profiles of the full cells with LFP as the cathode recorded at 1C. a) Li foil as the anode. b) The MXene/Li film as the anode.

Table S1. The electrochemical performance of the MXene/SiO_2 composite film is compared with most recent literatures about the MXene films.

Anode	Cathode	Current density	Voltage window	Cycling number	Capacity retention	Ref.
MXene/g-C_3N_4	LFP	0.5C	4.0-2.2 V	320	85.5%	*3*
MXene film	LFP	1C	3.8-2.5 V	80	87.7%	4
MXene@CNF	LFP	0.2C	3.8-2.0 V	200	94%	*5*
Mxene aerogel	LFP	1C	4.1-2.2 V	500	70.4%	6
MXene@Au	LFP	1C	3.8-2.5 V	200	98.47%	7
MXene (Nb_2C)	NCM	0.25C	4.3V-3 V	100	78%	8
B-doped MXene	LFP	0.5 C	3-0.05 V	35	90%	9
MXene/Si/C	LNMO	1C	5.0-3.5 V	300	95.52%	10
MXene/SiO_2 film	**LFP**	**3C**	**4.0-2.5 V**	**350**	**≈100%**	**This work**

Note：NCM: $LiNi_{1/3}Co_{1/3}Mn_{1/3}O_2$ and LNMO: $LiNi_{0.5}Mn_{1.5}O_4$

References:

[1] R. Pathak, K. Gurung, B.Bahrami, A.Wu, N. Ghimire, B. Zhou, W. Zhang, Y. Zhou, Q. Qiao, *Adv. Energy Mater.* **2019**, 9, 1901486.

[2] G. Lee, S. Kim, J. Choi, *Adv. Funct. Mater.* **2017**, 27, 1703538.

[3] F. Zhao, P. Zhai, Y. Wei, Z. Yang, Q. Chen, J. Zuo, X. Gu and Y. Gong, Adv. Sci., 2022, **9**, 2103930-2103941.

[4] C. Wei, H. Fei, Y. Tian, Y. An, H. Guo, J. Feng ,Y. Qian, Energy Storage Mater., 2020, **26**,223-233.

[5] C. Wang, Z. Zheng, Y. Feng, H. Ye, F. Cao , Z. Guo, Nano Energy, 2020, 74. 104817-104825.

[6] X. Meng, Y. Sun, M. Yu, Z. Wang , J. Qiu, Small Science, 2021, **1**. 2100021-2100030.

[7] Y. Qian, C. Wei, Y. Tian, B. Xi, S. Xiong, J. Feng , Y. Qian, Chem. Eng. J., 2021, **421**. 129685-129691.

[8] W. Zhang, H. Jin, Y. Du, G. Chen , J. Zhang, Electrochimica Acta, 2021, **390**. 138812-138817.

[9] N. Wu, Q. Zhang, Y. Guo, L. Zhou, L. Zhang, M. Wu, W. Wang, Y. Yin, P. Sheng , S. Xin, Rare Metals, 2022, **41**, 2217-2222.

[10] Y. An, Y. Tian, Y. Zhang, C. Wei, L. Tan, C. Zhang, N. Cui, S. Xiong, J. Feng , Y. Qian, ACS Nano, 2020, **14**, 17574-17588.